pp 983–1004. © Royal Aeronautical Society 2017
doi: 10.1017/aer.2017.51

Gimbaled-thruster based nonlinear attitude control of a small spacecraft during thrusting manoeuvre

Farhad Fani Saberi
f.sabery@aut.ac.ir
Space Science and Technology Institute
Amirkabir University of Technology
Tehran
Iran

Mansour Kabganian and Hamed Kouhi
Department of Mechanical Engineering
Amirkabir University of Technology
Tehran
Iran

Morteza Shahravi
Space Research Institute
Tehran
Iran

ABSTRACT

In this paper, a novel thrusting manoeuvre control scheme is proposed for a small spacecraft which is based only on the gimbaled thrust vector control (TVC) system. The spacecraft structure is composed of a body and a gimbaled thruster where common attitude control systems such as reaction control system (RCS) and spin stabilisation are not employed. A nonlinear two-body model is considered for the characterisation of the gimbaled-nozzle spacecraft where the gimbal actuator provides the only active control input. The spacecraft attitude is affected by a large exogenous disturbance torque which is generated by a thrust vector misalignment from the centre of mass (CM). To achieve some performance goals in the both transient and steady-state modes, a new control scheme is derived based on the combination of two linear and nonlinear controllers. The proposed method ensures the attitude and thrust vector stability during an impulsive orbital manoeuvre while eliminating and rejecting an exogenous disturbance torque. The numerical simulations illustrate the applicability of this method for using in a small spacecraft and its efficiency in sustained operation.

Received 28 October 2016; revised 21 April 2016; accepted 3 May 2017.

Keywords: impulsive orbital manoeuvre; thrust vector misalignment; gimbaled thruster; disturbance rejection; nonlinear attitude control

NOMENCLATURE

$\boldsymbol{\Delta v}$	velocity change increment
$x_s y_s z_s$	body-fixed coordinate frame
$x_n y_n z_n$	nozzle-fixed coordinate frame
$X_I Y_I Z_I$	inertial coordinate system
$\boldsymbol{\omega}_s$	body angular velocity
$\boldsymbol{\tau}_s$	body external torque
G_s	body CM location
G_n	nozzle CM location
$\boldsymbol{\omega}_n$	nozzle angular velocity
$\boldsymbol{\tau}_n$	nozzle external torque
F_T	thrust force
α	gimbal angle
$\boldsymbol{\omega}_r$	angular velocity of the nozzle with respect to the body
$\dot{\boldsymbol{\omega}}_r$	angular acceleration of the nozzle with respect to the body
$\dot{\boldsymbol{\omega}}_s$	spacecraft body angular acceleration
m_s	body mass
m_n	nozzle mass
θ	body attitude angle
J_d	jet damping coefficient
z_s	uncertainty in the body CM location
x_s	half of the body length
x_n	half of the nozzle length
Δv_d	desired velocity change
t_b	burning time
I_{s2}	body moment of inertia
I_{n2}	nozzle moment of inertia
α_{gimb}	maximum gimbal angle
δ_{FT}	thrust vector deviation from the X_I
u	control input
K	linear controller gain
P	closed-loop system poles
Δv_w	wasted velocity change
τ_d	exogenous disturbance
u_{com}	combined controller input
u_{lin}	linear controller input
u_{nonl}	nonlinear controller input

1.0 INTRODUCTION

Attitude control of a spacecraft during an impulsive thrusting manoeuvre has been a difficult problem since the early days of space missions. An impulsive orbital manoeuvre

https://doi.org/10.1017/aer.2017.51 Published online by Cambridge University Press

(i.e., retrofiring before an atmospheric re-entry) is used to generate a velocity increment $\boldsymbol{\Delta v}$ by using a large thrust force. During the burning of a rocket, thrust vector misalignment from the CM always exists and is inescapable[1]. This misalignment produces a large disturbance torque that tends to divert the orientation of spacecraft and thrust vector from the desired inertial direction. It is obvious that a high-capacity attitude control system is needed to compensate for the mentioned large exogenous disturbance. Since the spacecraft attitude during a thrusting manoeuvre is naturally unstable, desired values of $\Delta\mathbf{v}$ components cannot be achieved in practice. A review study about the effects of thrust vector misalignments on orbit transfers has been addressed in Ref. 2. The main control methods are classified in the NASA report[3] which are (1) spin-stabilisation for a small spacecraft (i.e. Biosatellite), (2) RCSs (in Mercury and Gemini), and (3) a combination of a RCS and TVC for large spacecraft (Apollo and Viking). In addition to the methods presented in Ref. 3, a novel method is proposed in Ref. 4 where the combination of the TVC scheme and spin-stabilisation is formulated and investigated.

A simple and low-cost method which is used in orbital manoeuvres of small satellites and spacecraft is spin stabilisation[5-7]. But it has some disadvantages and limitations:

1. Due to the flexibility and energy dissipation sources in a spacecraft, only the spin about the axis of maximum moment of inertia is stable for a spin-stabilised-only spacecraft.
2. Nutational or coning instability has happened in several spacecraft therefore, a nutation control system equipped with a RCS is needed[8-10].
3. Some equipment such as thrusters and fuel tanks are needed for spin-up and spin-down[3].
4. In some works such as in Refs 11-13, the resonance in the spacecraft devices created by the nutation is addressed.
5. Spin-axis stabilisation (thrust vector stabilisation) with respect to the desired inertial direction is not possible for a spin-stabilised-only spacecraft. In the some works such as Refs 14-17, it is shown that for the spin-axis stabilisation, an active control system with extra actuators (such as RCSs) is needed.
6. Spin stabilisation may not be a suitable choice for a spacecraft with solar panels, directional antennae and sensors which are sensitive to angular motions, especially in a lengthy mission.

An RCS is able to provide a high level of active control torque to reject exogenous disturbances and perform fast attitude manoeuvres. Although RCSs have many advantages, in practice they have many weaknesses and limitations such as:

1. They include several pieces of equipment that increase the complexity and cost of a spacecraft
2. Because RCSs use liquid propellants, fuel sloshing occurs due to rotational and lateral motions of propellant tanks; in the presence of sloshing, attitude control of spacecraft will be very difficult. There are several works such as Refs 18-21 on the interaction of spacecraft dynamics and slosh dynamics and their control. In Refs 18 and 22-24, the TVC for the rocket engine is addressed, including the fuel slosh dynamics in which many external torques are needed in the control system.
3. RCSs are inherently nonlinear actuators with complex control logic[25]. Although for large spacecraft and upper-stage vehicles (see Refs 1, 18 and 26-28) a combination of

https://doi.org/10.1017/aer.2017.51 Published online by Cambridge University Press

RCSs and TVC has been employed, RCSs are not suitable to be used in a small spacecraft mission.

The TVC method with all its advantages is a powerful technique in control of spacecraft and launchers which can be actuated by a servo actuator (without fuel consumption). For instance, terminal guidance and landing capability of the Falcon 9 rocket with new TVC system technology is being provided by the company SpaceX. Although during an impulsive manoeuvre, a high-level disturbance torque is created proportional to the thrust vector misalignment, a gimbaled TVC can generate an active control torque larger than the disturbance level. When the disturbance level is larger than the attitude control capacity, a fixed thrust system is not efficient (Apollo, Cassini[29], [30] and rockets). TVC methods such as moving plates[31] are accompanied by a highly nonlinear behaviour in comparison with the gimbaled thruster. A gimbaled TVC can be also employed for a solar-sail spacecraft[32]. The gimbaled nozzle (gimbaled thruster) can be very useful in preserving weight, simplifying the attitude control system and reducing the requirements of the CM positioning accuracy[3,4,28]. It should be noted that in large and massive spacecraft or launchers with a liquid propellant rocket, several heavy and complex components as well as fuel tanks are located in the body not presented (or attached) at the rotatable nozzle. Therefore, the mass properties of the liquid propellant rocket are negligible in comparison with the body's, and as a result, the dynamical interaction between the movable nozzle and body will be very small[1,18,22,23]. It is obvious that using a liquid propellant rocket is not efficient or possible for a small spacecraft for which a SRM (solid rocket motor) is used where all mass properties of the SRM (including solid fuel) will be added to the nozzle mass properties. Therefore, for a small spacecraft equipped with a SRM, the aforementioned interaction cannot be neglected and leads to nonlinear two-body dynamics[4,28,33]. Note that for large spacecraft, a TVC was used together with RCSs[1,18,26,27] and for a small spacecraft, it has been combined with the spin-stabilisation method[4]. Although in Felicetti et al[34], an adaptive thrust vector control during on-orbit servicing is addressed, the interaction dynamics between the nozzle and the body is not considered as well, because it is not applicable for an impulsive orbital manoeuvre. In Wang et al[28], a nonlinear control law based on a two-axis gimbaled thruster is proposed for an upper-stage launcher where the launcher is equipped with eight RCSs on the body and two gimbal actuators by which the nonlinear dynamics is over-actuated. In contrast to Wang[28], the control of an underactuated system is investigated in this paper.

The use of momentum exchange devices such as reaction wheels and control moment gyros for attitude control is very attractive because, they do not require any fuel consumption. The external disturbance rejection is not possible for an attitude control system based only on these devises. In study[33], a large control torque has been produced by the interaction between the reaction wheels angular momentum and the spacecraft spin rate, but in this paper the use of these devices is deficient.

Some major assumptions and goals that establish the control problem of this paper are considering of 1) a small spacecraft 2) the nonlinear two-body dynamics model 3) an impulsive orbital manoeuvre (high velocity change in a short time) with a high level exogenous disturbance 4) using only gimbal actuator and 5) not using of the RCS and spin-stabilisation (because of their limitations). Although attitude control during thrusting manoeuvre has received a large attention, it is clear that up to now, only TVC method has not been used to solve the mature problem in hand. The exogenous disturbance torque originates from the CM location uncertainty, is much more than the other orbital disturbance sources such as drag, solar pressure, and earth oblate disturbance. The difficulty of the present control problem

https://doi.org/10.1017/aer.2017.51 Published online by Cambridge University Press

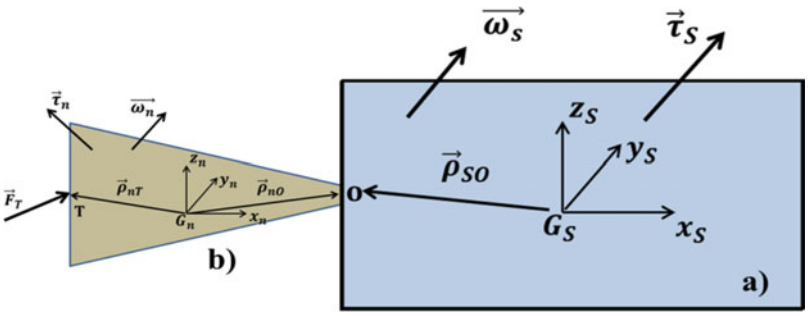

Figure 1. (Colour online) A small spacecraft composed of body (a), nozzle (b) and a gimbal actuator at the pivot o.

is that for the two-body nonlinear plant, both attitude and thrust vector stabilisation (with respect to the desired inertial direction Z_I) must be performed using only a gimbal actuator while rejecting the exogenous disturbance torque. According to the previous literatures, these performances need some thrusters (RCSs) and fuel consumption which are not efficient for a small spacecraft. Similar to[33], in this paper a small spacecraft equipped with a gimbaled-SRM is considered in which the nozzle mass properties are not negligible with respect to the body's. Although orbital manoeuvres are performed in a three dimensional space, in some papers such as Reyhanoglu and Hervas[18], a planar manoeuvre is considered in order to facilitate the stability analysis. In this paper, a planar manoeuvre is also considered. To achieve some performance goals in transient and steady-state modes, a new control scheme is derived based on combination of two linear and nonlinear controllers. The proposed method ensures attitude and thrust vector stability during an impulsive orbital manoeuvre while eliminating and rejecting the exogenous disturbance torque. The important control object which is considered for the transient mode is to stabilise the body attitude angle very fast and in an under-damped behaviour without any overshoot and oscillation. The damped behaviour of the body attitude is very useful and effective for a flexible spacecraft (i.e., one equipped with solar panels).

The remainder of the paper is organised as follows. In Section 2 the planar dynamics model of a small spacecraft equipped with a gimbaled-nozzle is achieved. In Section 3, the proposed control system including linear, nonlinear and combined controllers is designed along with its simulation results. In Section 4, the important findings are discussed, and the conclusion is reported in Section 5.

2.0 MODEL FORMULATION

As discussed before, in the modelling of the spacecraft, the dynamical interaction between the nozzle and body must be considered. As indicated in Fig. 1, the spacecraft is composed of the three main parts: the body, the nozzle and the gimbal where the nozzle can rotate by means of a gimbal actuator at the pivot o. Subscripts s, n, o and T denote the body, nozzle, gimbal pivot and point of acting the thrust force, respectively. $x_s y_s z_s$ is the body-fixed coordinate frame (x_s is parallel to the body longitudinal axis), G_s denotes the body CM location, $\boldsymbol{\tau}_s \in \boldsymbol{R}^3$ and $\boldsymbol{\omega}_s \in \boldsymbol{R}^3$ express the body external torque and the angular velocity respectively, $\boldsymbol{\rho}_{so} \in \boldsymbol{R}^3$ is the vector from G_s to the gimbal pivot, G_n is the nozzle CM position, $x_n y_n z_n$ is the nozzle-fixed coordinate frame, and $\boldsymbol{\tau}_n \in \boldsymbol{R}^3$ and $\boldsymbol{\omega}_n \in \boldsymbol{R}^3$ represent the nozzle external torque and the angular velocity, respectively. The control input is defined by the gimbal angles of a

https://doi.org/10.1017/aer.2017.51 Published online by Cambridge University Press

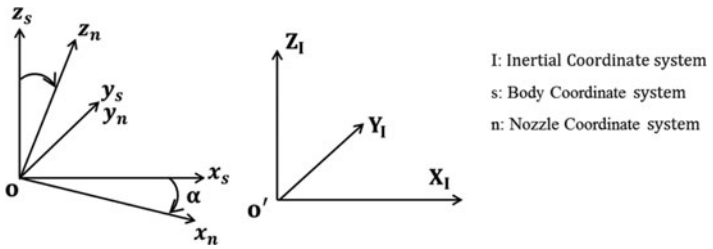

Figure 2. The gimbal rotation at the pivot o and the body, nozzle and inertial coordinate system.

non-throttable thrust engine (F_T) without any other moment source. The gimbal deflects the thrust vector with respect to the spacecraft's CM and then the attitude control torque is produced in proportion to the thrust vector misalignment.

2.1 Nonlinear dynamics of the planar manoeuvre

In the planar manoeuvre, the rotations are around the y_s (y_n) axis. The nozzle rotation with respect to the body and inertial coordinate system is shown in Fig. 2 with gimbal angle α. Thus, the relative angular velocity and acceleration of the nozzle with respect to the body will be $\boldsymbol{\omega}_r = [0\ \dot{\alpha}\ 0]^T$, $\dot{\boldsymbol{\omega}}_r = [0\ \ddot{\alpha}\ 0]^T$.

The corresponding rotation matrix that transforms a vector in the nozzle frame to a vector in the body frame is

$$\boldsymbol{R}_n^s(\alpha) = \begin{bmatrix} \cos(\alpha) & 0 & \sin(\alpha) \\ 0 & 1 & 0 \\ -\sin(\alpha) & 0 & \cos(\alpha) \end{bmatrix} \quad \ldots(1)$$

The three-dimensional mathematical modelling of a two-body spacecraft is derived in Ref. 33 by which $\dot{\boldsymbol{\omega}}_s$ as the spacecraft body angular acceleration can be calculated as

$$\begin{aligned} \dot{\boldsymbol{\omega}}_s = [\boldsymbol{I}_{ns,T}]^{-1} \big[& \boldsymbol{\tau}_{ns} + \boldsymbol{\rho}_T \times \boldsymbol{F}_T - \boldsymbol{I}_r(\dot{\boldsymbol{\omega}}_r + \boldsymbol{\omega}_s \times \boldsymbol{\omega}_r) \\ & + M\boldsymbol{\rho}_{ns} \times (\boldsymbol{\omega}_s \times (\boldsymbol{\omega}_s \times \boldsymbol{\rho}_{so}) - \boldsymbol{\omega}_n \times (\boldsymbol{\omega}_n \times \boldsymbol{\rho}_{no})) \\ & - \boldsymbol{\omega}_s \times (\boldsymbol{I}_s\boldsymbol{\omega}_s) - \boldsymbol{\omega}_n \times (\boldsymbol{I}_n\boldsymbol{\omega}_n) \big] \end{aligned} \quad \ldots(2)$$

where $\boldsymbol{\omega}_s = [\omega_{sx}\ \omega_{sy}\ \omega_{sz}]^T$, $\boldsymbol{\omega}_n = \boldsymbol{\omega}_s + \boldsymbol{\omega}_r$, $\boldsymbol{\tau}_{ns} = \boldsymbol{\tau}_s + \boldsymbol{\tau}_n$, $\boldsymbol{\rho}_{ns} = \boldsymbol{\rho}_{no} - \boldsymbol{\rho}_{so}$, $\boldsymbol{\rho}_{sn} = -\boldsymbol{\rho}_{ns}$. $\boldsymbol{I}_s \in \boldsymbol{R}^{3\times3}$ and $\boldsymbol{I}_n^n \in \boldsymbol{R}^{3\times3}$ are the body and the nozzle moment of inertia, respectively. m_s and m_n are the body and the nozzle mass, by which $M = (m_n m_s)/(m_n + m_s)$, $\boldsymbol{I}_{ns,T} = \boldsymbol{I}_{ns} - M[\boldsymbol{\rho}_{ns}\times]^2$, $\boldsymbol{I}_r = \boldsymbol{I}_n - M[\boldsymbol{\rho}_{ns}\times][\boldsymbol{\rho}_{no}\times]$, $\boldsymbol{\rho}_T = \boldsymbol{\rho}_{nT} + \boldsymbol{\rho}_{sn}(M/m_n)$, $\boldsymbol{I}_{ns} = \boldsymbol{I}_s + \boldsymbol{I}_n$. All vectors and moment of inertias are presented in the s frame. For a vector $\boldsymbol{s} = [s_1\ s_2\ s_3]^T$, the operator $[\boldsymbol{s}\times]$ is defined by

$$[\boldsymbol{s}\times] = \begin{bmatrix} 0 & -s_3 & s_2 \\ s_3 & 0 & -s_1 \\ -s_2 & s_1 & 0 \end{bmatrix}$$

Some assumptions and definitions are made to summarise and extract the planar manoeuvre mathematical model from the three-dimensional modelling of Equation (2).

The attitude of the body is the rotation angle θ around the y_s axis with angular velocity $\omega_{sy} = \dot{\theta}$ that results in $\boldsymbol{\omega}_s = [0\ \dot{\theta}\ 0]^T$. As assumed before, there is no external control torque

https://doi.org/10.1017/aer.2017.51 Published online by Cambridge University Press

($\boldsymbol{\tau}_s = \mathbf{0}_{3\times1}$) and the only active control input is $\ddot{\alpha}$ (in $\dot{\boldsymbol{\omega}}_r$); no attitude control torque exists that directly controls the spacecraft attitude. Some parameters and inputs are given in Equation (3) where $J_d(\dot{\alpha}+\dot{\theta})$ denotes the passive torque created by the jet damping effect and J_d is the damping coefficient. The jet-damping torque originates from the Coriolis forces due to the outflow of SRM gases; a detailed discussion on the jet damping can be found in Refs 35 and 36. In vector $\boldsymbol{\rho}_{so}$, z_s represents the uncertainty in the CM location that leads to thrust vector misalignment (offset) and produces the exogenous disturbance torque.

$$\begin{aligned}
&\boldsymbol{\rho}^n_{no} = \begin{bmatrix} x_n & 0 & 0 \end{bmatrix}^T,\ \ \boldsymbol{\rho}^n_{nT} = 0_{3\times1},\ \ \boldsymbol{\rho}_{so} = \begin{bmatrix} -x_s & 0 & z_s \end{bmatrix}^T,\\
&\boldsymbol{I}^n_n = diag(I_{n,11}\,,\ I_{n,22},\ I_{n,33}),\ \ \boldsymbol{I}_s = diag(I_{s,11}\,,\ I_{s,22},\ I_{s,33}),\\
&\mathbf{F}^n_T = \begin{bmatrix} \bar{F}_T & 0 & 0 \end{bmatrix}^T,\ \ \boldsymbol{\tau}_n = \begin{bmatrix} 0 & -J_d(\dot{\alpha}+\dot{\theta}) & 0 \end{bmatrix}^T
\end{aligned} \quad \ldots(3)$$

Actually, the magnitude of the thrust offset z_s is so much smaller than the dimensions of the spacecraft's body and nozzle, it then can be assumed that

$$z_s << x_n,\ \ z_s << x_s \quad \ldots(4)$$

Thus, under the indicated assumptions and considerations, the nonlinear dynamics of the planar manoeuvre in the y axis is given in Equation (5) where $d_X z_s$ and u denote the disturbance acceleration and the control input, respectively. During the engine burn, the undesired transverse acceleration $d_X z_s$, produces the undesired velocity. The details of the nonlinear terms f_X and d_X and the two moments of inertia $I_r(\alpha)$ and $I_{yy}(\alpha)$ are given in Equations (6) and (7), respectively.

$$\begin{aligned}
&\ddot{\theta} = f_X - {I_r(\alpha)}/{I_{yy}(\alpha)}\ u + d_X z_s,\\
&\ddot{\alpha} = u.
\end{aligned} \quad \ldots(5)$$

$$\begin{cases}
f_X = -\frac{\bar{F}_T M}{m_n I_{yy}(\alpha)} x_s \sin(\alpha) + \frac{M x_s x_n}{I_{yy}(\alpha)} \sin(\alpha)(\dot{\alpha}^2 + 2\dot{\alpha}\dot{\theta}) - \frac{J_d(\dot{\alpha}+\dot{\theta})}{I_{yy}(\alpha)},\\
d_X = \frac{M}{I_{yy}(\alpha)}\left(\frac{\bar{F}_T}{m_n} - x_n(\dot{\alpha}^2 + 2\dot{\alpha}\dot{\theta})\right) cos(\alpha).
\end{cases} \quad \ldots(6)$$

$$\begin{aligned}
&I_r(\alpha) = I_{n,\ 22} + M x_n^2 + M x_s x_n \cos(\alpha) + M x_n z_s sin(\alpha),\\
&I_{yy}(\alpha) = I_{n,\ 22} + I_{s,\ 22} + M(x_s + x_n cos(\alpha))^2 + M(z_s + x_n sin(\alpha))^2
\end{aligned} \quad \ldots(7)$$

2.2 Mission requirements and parameters

The purpose of this section is to define the spacecraft mission requirements and parameters. Since the aim is to show the specifications of the proposed method and compare it with the other thrusting methods, a typical mission is considered here which is similar to the deorbiting manoeuvre of some small spacecraft. The goal of this mission is to generate a large $\Delta \boldsymbol{v}$ in a short time for performing an impulsive orbital manoeuvre. Based on this mission, the specifications of the proposed method are obtained, and its merits and weaknesses will then be compared with the other methods. Because a comparative study will be done here, it is not necessary to define an absolute accuracy for the orbital mission. Moreover, in space engineering, one cannot generally say that one method is better than another method; based on various mission requirements and criteria, design procedures should be passed and finally the better case may be determined. Therefore, in this paper according to some special criteria

https://doi.org/10.1017/aer.2017.51 Published online by Cambridge University Press

Table 1
The spacecraft parameters

Δv_d(m/s)	t_b(s)	$\bar{F}_T$	J_d(Nm.s)	z_s(cm)	$I_{s2}(kgm^2)$	$I_{n2}(kgm^2)$	$m_s(kg)$	$m_n(kg)$	$x_n(m)$	$x_s(m)$
100	15	1053N	2	4	10	1	150	8	0.2	0.75

(not generally), the proposed method is compared with the other thrusting method. Moreover, the attempt is to show that the proposed method is able to satisfy the objectives of this paper.

The impulsive orbital transfer mission is defined by the desired velocity change Δv_d and a short burning time t_b. Similar to deorbiting missions of some spacecraft, a large $\Delta v_d = 100$m/s is selected and the short burning time is chosen to be $t_b = 15s$. The small spacecraft body parameters selected are $m_s = 150\,kg$, $x_s = 0.75m$ and $I_{s2} = 10$ kgm^2. Based on an SRM burning specification, the nozzle's mass is approximately $m_n = 8kg$ and finally the thrust force can be calculated as $\bar{F}_T = (m_n + m_s)(\Delta v_d / t_b) = 1053$N. The other nozzle parameters selected are $x_n = 0.2\ m$ and $I_{n2} = 1\,kgm^2$. Maximum offset in the CM location is considered as $z_s = 4$ cm (more than the value in Ref. 10). Finally, the jet damping coefficient is considered as $J_d = 2\,Nms$. The parameters are listed in Table 1.

Due to the mechanical limitation and necessity for a good thrusting manoeuvre performance, the nozzle deviation should not be larger than an inappropriate value. The maximum value of gimbal angle is considered to be bounded by

$$|\alpha(t)| < \alpha_{gimb}\,, \qquad \ldots (8)$$

by which the following approximation can be concluded:

$$\begin{aligned} \bar{I}_r &\approx I_{n,\,22} + M x_n (x_n + x_s), \\ \bar{I}_{yy} &\approx I_{n,\,22} + I_{s,\,22} + M(x_s + x_n)^2 \end{aligned} \qquad \ldots (9)$$

It should be noted that the closed-loop control system must meet and satisfy the condition (8).

3.0 CONTROLLER DESIGN

This section presents a detailed development of three types feedback control law through the nonlinear model obtained in Equation (5). First, the control problem statement is presented and then a linear controller with controllability analysis is designed. Next, in order to modify some weaknesses of the linear controller in transient mode, a nonlinear control law is proposed in which the stability of the nonlinear closed-loop system is proved. Finally, both linear and nonlinear controllers are combined together in order to achieve an efficient controller which is better than the two aforementioned controllers.

3.1 Control problem statement

For the planar manoeuvre, the linear acceleration components of the spacecraft CM in the inertial coordinate system ($X_I Y_I Z_I$ in Fig. 2), is given in Equation (10) where $\delta_{FT} = \alpha + \theta$ is the thrust vector deviation from the desired inertial direction X_I; v_x, v_z are the axial and transverse components, respectively, of the velocity change of the CM;

https://doi.org/10.1017/aer.2017.51 Published online by Cambridge University Press

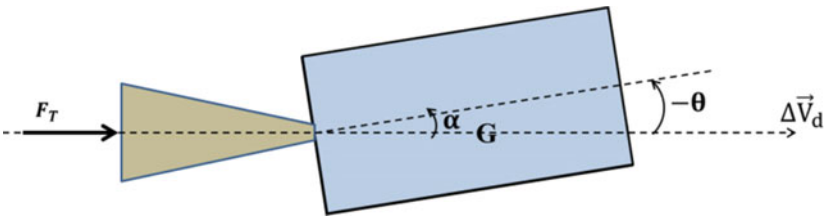

Figure 3. (Colour online) The desired equilibrium condition of the spacecraft in presence of CM uncertainty.

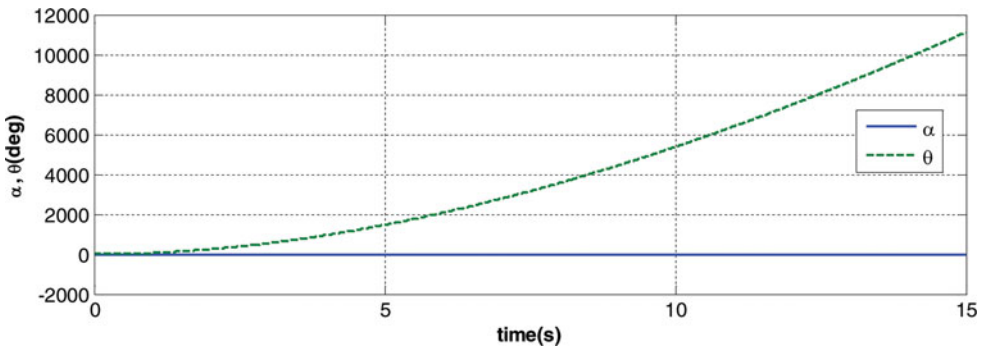

Figure 4. (Colour online) Spacecraft body attitude (θ) and gimbal angle (α) without active control.

and $a_{\max} = \bar{F}_T/(m_s + m_n)$ represents the maximum acceleration.

$$\begin{aligned} \dot{\mathrm{v}}_x &= a_{\max}\cos(\delta_{FT}), \\ \dot{\mathrm{v}}_z &= -a_{\max}\sin(\delta_{FT}) \end{aligned} \qquad \ldots(10)$$

As discussed before, the control object is to eliminate the undesired acceleration component ($\dot{\mathrm{v}}_z \to 0$) in order to maximise the velocity change in the $\mathrm{X_I}$ direction ($\dot{\mathrm{v}}_x \to a_{\max}$). Therefore, in addition to the attitude stabilisation, the important consideration is to direct the thrust vector F_T toward the inertial $\mathrm{X_I}$ direction or to achieve $\delta_{FT,eq} = \theta_{eq} + \alpha_{eq} \to 0$ as time tends to infinity. If there is the offset z_s in the CM location, then the desired equilibrium condition of the spacecraft can be shown in Fig. 3. The control system must align the thrust vector through the spacecraft CM (G) and desired velocity change $\Delta\mathbf{v_d}$ direction ($\mathrm{X_I}$) simultaneously. To reach these objects, the stabilised state variables will be

$$\theta_{eq} = -\alpha_{eq}, \quad \dot{\theta}_{eq} = \dot{\alpha}_{eq} = 0 \qquad \ldots(11)$$

Using Equations (5), (6) and (4), θ_{eq} and α_{eq} are obtained in Equation (12).

$$\begin{aligned} &\ddot{\theta} = 0,\ \dot{\theta} = 0,\ \dot{\alpha} = 0,\ u = 0, \\ &\Rightarrow f_X + d_X z_s = 0, \\ &\Rightarrow -\tfrac{\bar{F}_T M}{m_n I_{yy}(\alpha_{eq})} x_s \sin(\alpha_{eq}) + \tfrac{M}{I_{yy}(\alpha_{eq})}\left(\tfrac{\bar{F}_T}{m_n}\right) cos(\alpha_{eq})\, z_s = 0 \quad \Rightarrow \tan(\alpha_{eq}) = \tfrac{z_s}{x_s}\ , \\ &\Rightarrow\ \alpha_{eq} \approx z_s/x_s\ \ \&\ \ \theta_{eq} \approx -z_s/x_s. \end{aligned} \qquad \ldots(12)$$

https://doi.org/10.1017/aer.2017.51 Published online by Cambridge University Press

Thrust vector misalignment must be completely rejected by the proper gimbal deflection (see Fig. 3). In what follows, it is assumed that z_s is constant[24] and can be estimated by a nonlinear disturbance observer[37,38].

To obtain a stabilisation control problem, the error dynamics are needed, for which new variables are defined as

$$\bar{\theta} = \theta - \theta_{eq}\,, \quad \bar{\alpha} = \alpha - \alpha_{eq} \qquad \ldots(13)$$

Using Equations (4), (12), (9) and (13), the form of the nonlinear plant in Equations (5) and (6) are changed into Equation (14).

$$\begin{aligned} \ddot{\bar{\theta}} &= \bar{f}_X - (\bar{I}_r/\bar{I}_{yy})u, \\ \ddot{\bar{\alpha}} &= u, \end{aligned} \qquad \ldots(14)$$

where $\bar{f}_X = -\frac{\bar{F}_T M}{m_n \bar{I}_{yy}} x_s \sin(\bar{\alpha}) + \frac{M x_s x_n}{\bar{I}_{yy}} \sin(\bar{\alpha})(\dot{\bar{\alpha}}^2 + 2\dot{\bar{\alpha}}\dot{\bar{\theta}}) - \frac{J_d(\dot{\bar{\alpha}}+\dot{\bar{\theta}})}{\bar{I}_{yy}}$

3.2 Linear controller design

In this section, at first controllability of the proposed method near the equilibrium point will be investigated and then a linear controller will be designed to result in a steady-state response.

3.2.1 Controllability of the linearised system

Before designing a linear or nonlinear control law, the controllability analysis of the linearised system is important to show the behaviour of the nonlinear system near the equilibrium point. By linearising the plant (Equation 14) about $\bar{\theta} = 0$ and $\bar{\alpha} = 0$, the linear model is derived and given by

$$\begin{aligned} \ddot{\bar{\theta}} &= -\frac{\bar{F}_T M}{m_n \bar{I}_{yy}} x_s \bar{\alpha} - \frac{J_d(\dot{\bar{\alpha}}+\dot{\bar{\theta}})}{\bar{I}_{yy}} - \frac{\bar{I}_r}{\bar{I}_{yy}} u, \\ \ddot{\bar{\alpha}} &= u. \end{aligned} \qquad \ldots(15)$$

By introducing $\boldsymbol{X} = [\bar{\theta}\ \dot{\bar{\theta}}\ \bar{\alpha}\ \dot{\bar{\alpha}}]^T$ as the vector of state variables, the linear state space model is given as

$$\dot{\boldsymbol{X}} = \boldsymbol{A}\boldsymbol{X} + \boldsymbol{B}u, \qquad \ldots(16)$$

where $\boldsymbol{A} = \begin{bmatrix} 0 & 1 & 0 & 0 \\ 0 & -\frac{J_d}{\bar{I}_{yy}} & -\frac{\bar{F}_T M}{m_n \bar{I}_{yy}} x_s & -\frac{J_d}{\bar{I}_{yy}} \\ 0 & 0 & 0 & 1 \\ 0 & 0 & 0 & 0 \end{bmatrix}$, $\boldsymbol{B} = \begin{bmatrix} 0 \\ -\frac{\bar{I}_r}{\bar{I}_{yy}} \\ 0 \\ 1 \end{bmatrix}$

The controllability matrix Co is formed here in which the rank condition $|\boldsymbol{Co}| \neq 0$ is guaranteed. Therefore, the origin of the linearised system can be made uniformly asymptotically stable by a linear state feedback.

$$\boldsymbol{Co} = [\boldsymbol{B}, \boldsymbol{AB}, \boldsymbol{A^2B}, \boldsymbol{A^3B}],\ |\boldsymbol{Co}| = \frac{\bar{F}_T M x_s (\bar{F}_T \bar{I}_{yy}^2 M x_s + m_n J_d^2 (\bar{I}_r - \bar{I}_{yy}))}{(\bar{I}_{yy}^2 m_n)^2}$$

https://doi.org/10.1017/aer.2017.51 Published online by Cambridge University Press

If the pair (A, B) be controllable, then the following controller can guarantee the stability of the above system:

$$u(t) = -\boldsymbol{K}\boldsymbol{X}(t), \boldsymbol{K} \in R^{1\times n} \quad \ldots(17)$$

This type of controller is the preferred for many industrial applications. By using a proper gain $\boldsymbol{K}$, $\tilde{\boldsymbol{A}} = \boldsymbol{A} - \boldsymbol{B}\boldsymbol{K}$ can be stable. To have a good response at first, poles location are selected then MATLAB place function is used to compute gain $\boldsymbol{K}$ from the mentioned poles.

3.2.2 Numerical simulation

In this subsection, the simulation results of the nonlinear plant with a linear controller are carried out. The objects are to show the merits and weaknesses of using the linear controller in the proposed method. The time response specifications which are studied here are transient and steady-state responses of the body and the gimbal angles and the overshoot of the body attitude. The set of parameters which are used in the simulations are listed in Table 1. The disturbance torque is $\tau_d = F_T z_s = 42.13\,\text{Nm}$. The poles location of the linearised closed-loop system is selected as $\boldsymbol{P}$ = (–1 + 0.5i, –1 –0.5i, –2 –0.8i, –2 + 0.8i) that results in the control gain $\boldsymbol{K}$ = (–0.138, –0.304, 13.182, 5.846). Simulations are done using MATLB/Simulink.

From Equation (10) Δv_x as the actual velocity change along the desired inertial direction X_I can be calculated as follows. The ideal condition at the thrusting manoeuvre is that $\delta_{FT}(t) = 0$ for $0 \le t \le t_b$ (or $\Delta v_x = \Delta v_d$).

$$\Delta v_x = \int_0^{t_b} a_{\max} \cos(\delta_{FT}(t))\, dt$$

Δv_z as the undesired velocity change component in the inertial direction Z_I can be calculated as

$$\Delta v_z = -\int_0^{t_b} a_{\max} \sin(\delta_{FT}(t))\, dt$$

However, the actual wasted velocity change is computed as

$$\Delta v_w = (\Delta v_d^2 - \Delta v_x^2)^{0.5}$$

The following two numerical simulations are carried out, which are the simulations of the open-loop system (without active control system) and the nonlinear system with the linear controller, respectively.

Case 1

In this case, the gimbal actuator is inactivated and fixed at $\alpha(t) = 0$. The attitude instability is obvious under the thrust vector misalignment ($z_s = 4$ cm or $\alpha_{eq} = 3^0$). This simulation shows that without an active controller, the disturbance $\tau_d = 42.13$Nm can rotate the thrust vector direction more than 1500° in the first 5 s. In the open loop mode, the orbital manoeuvre cannot be performed correctly. This simulation shows that a high-capacity control system (a high-level control torque during the burning time) is needed for an impulsive orbital manoeuvre.

https://doi.org/10.1017/aer.2017.51 Published online by Cambridge University Press

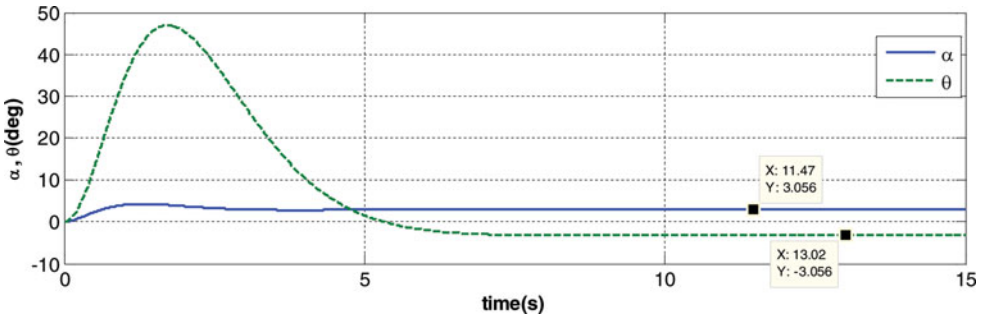

Figure 5. (Colour online) Spacecraft body attitude (θ) and gimbal angle (α) when using a linear controller.

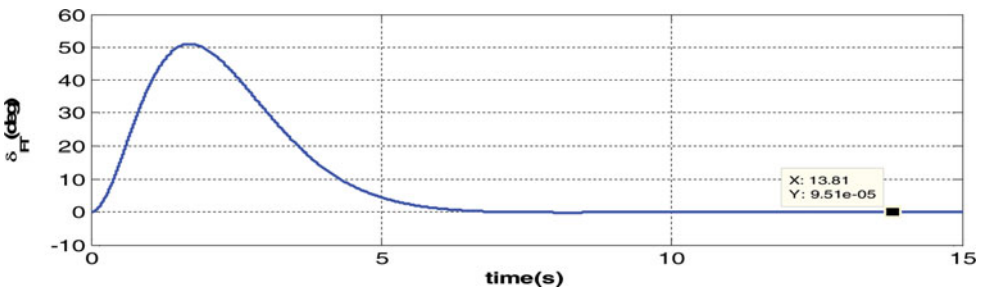

Figure 6. (Colour online) Thrust vector deviation (δ_{FT}) from the desired inertial direction (X_I) when using a linear controller.

Case 2

The simulation results of the closed-loop system with the linear controller are given in this case. In Fig. 5, the time response of the body and gimbal angle are presented while they are converging to $\theta_{eq} = -3.055°$ and $\alpha_{eq} = 3.055^0$, respectively. This result confirms the desired equilibrium condition in Fig. 3 where the thrust vector is pointed to the CM. Thrust vector stabilisation can be observed in Fig. 6 that converges to zero. Spacecraft velocity change along the two inertial directions is shown in Fig. 7. The velocity change along the axis X_I is $\Delta v_x = 95.27 m/s$ and the wasted velocity change is become $\Delta v_w = 30.38$ m/s.

The advantages of using the linear controller are:

1. After the transient time or in steady-state mode, thrust vector deviation is completely eliminated.
2. The control action in steady-state mode is zero while a high-level exogenous disturbance torque ($\tau_d = 42.13$Nm) is completely rejected.
3. Near the equilibrium point (where a linearised model is a good approximation,) the closed-loop system has a fast response to reach the steady-state mode.

The weaknesses of using the linear controller are:

1. High overshoot of the body attitude during the transient response (the damped behaviour is not achieved).

https://doi.org/10.1017/aer.2017.51 Published online by Cambridge University Press

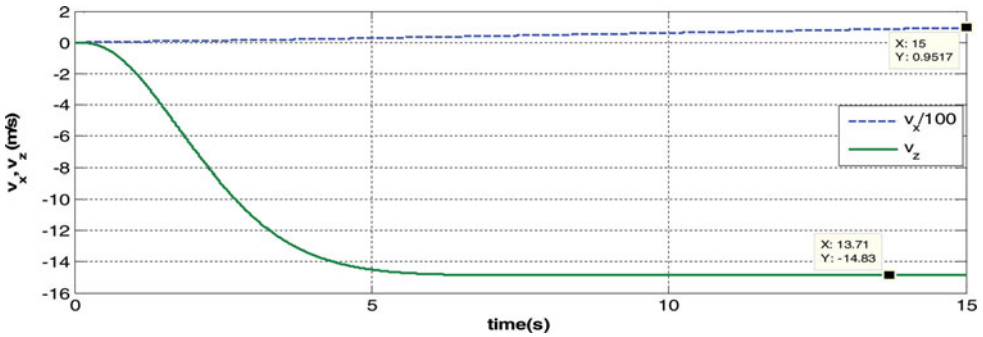

Figure 7. (Colour online) Spacecraft velocity change along the two inertial directions X_I and Z_I.

2. Duo to high deviation of the body attitude and consequently a high deviation of the thrust vector, much velocity change is wasted.
3. In the presence of the nonlinear terms (far from the equilibrium point), there is no stability analysis for the nonlinear closed-loop system.

3.3 Nonlinear controller design

In the previous section, a linear controller is designed and its weaknesses and merits are discussed. Here the object is to design a nonlinear controller that lacks the shortcomings of the linear controller. The purposes of the nonlinear control law are 1) a damped (or under-damped) behaviour without an overshoot can be achieved for the body attitude in the transient mode, and 2) to show the stability of the nonlinear closed-loop system.

At the following, at first a nonlinear control law is proposed next, the stability of the nonlinear closed-loop system is proven and then by using the numerical simulations, its lack and merits are explained.

3.3.1 Nonlinear control law

By introducing the scalars η, γ and ξ, and using $\bar{f}_X$, Equation (14) is reformed to Equation (18)

$$\begin{aligned}(\bar{I}_{yy}/\bar{I}_r)\ddot{\bar{\theta}} &= \left(-\eta + \gamma(\dot{\bar{\alpha}}^2 + 2\dot{\bar{\alpha}}\dot{\bar{\theta}})\right)\sin(\bar{\alpha}) - \xi(\dot{\bar{\alpha}} + \dot{\bar{\theta}}) - u,\\ \ddot{\bar{\alpha}} &= u,\end{aligned} \quad \ldots(18)$$

where $\eta = (\bar{F}_T M x_s)/(m_n \bar{I}_r)$, $\gamma = (M x_s x_n)/\bar{I}_r$, $\xi = J_d/\bar{I}_r$.

As noticed before, in addition to guarantee the stability of the nonlinear closed-loop system, the important goal is to achieve a smooth or damped behaviour for the body attitude θ. Therefore, first a compensator is design for regulating the angle θ in a damped manner and then the nonlinear stability of the gimbal angle α will be proven. By proposing the nonlinear control law in Equation (19), the nonlinear closed-loop system is achieved in Equation (20):

$$u = \left(-\eta + \gamma(\dot{\bar{\alpha}}^2 + 2\dot{\bar{\alpha}}\dot{\bar{\theta}})\right)\sin(\bar{\alpha}) - \xi(\dot{\bar{\alpha}} + \dot{\bar{\theta}}) - (\bar{I}_{yy}/\bar{I}_r)\ddot{\bar{\theta}}_r \quad \ldots(19)$$

https://doi.org/10.1017/aer.2017.51 Published online by Cambridge University Press

$$\begin{cases} \ddot{\bar{\theta}} = \ddot{\bar{\theta}}_r \,, \\ \ddot{\bar{\alpha}} = \left(-\eta + \gamma(\dot{\bar{\alpha}}^2 + 2\dot{\bar{\alpha}}\dot{\bar{\theta}})\right)\sin(\bar{\alpha}) - \xi(\dot{\bar{\alpha}} + \dot{\bar{\theta}}) - (\bar{I}_{yy}/\bar{I}_r)\ddot{\bar{\theta}}_r \,, \end{cases} \quad \ldots(20)$$

where

$$\ddot{\bar{\theta}}_r = -2\lambda\,\dot{\bar{\theta}} - \lambda^2\,\bar{\theta} \quad \ldots(21)$$

Putting Equation (21) into (Equation 20), the stable error dynamics of the $\bar{\theta}(t)$ are obtained in Equation (22) as

$$\ddot{\bar{\theta}} + 2\lambda\,\dot{\bar{\theta}} + \lambda^2\,\bar{\theta} = 0 \,, \quad \ldots(22)$$

where the constant and positive parameter $\lambda$is employed for tuning the convergence rate in a damped manner. Then the following result can be easily concluded:

$$\bar{\theta}(t) \to 0,\ \dot{\bar{\theta}}(t) \to 0\ \ \&\ \ \ddot{\bar{\theta}}_r \to 0 \quad as \quad t \to \infty \quad \ldots(23)$$

According to the outcomes of (23), some terms in Equation (20) can be neglected for $t > T_{ss}$ where T_{ss} is the settling time of the body attitude, which depends on the magnitude of λ. For $t = T_{ss}$, we have $\bar{\theta}(T_{ss}) \approx 0$ and $\dot{\bar{\theta}}(T_{ss}) \approx 0$; therefore, the stability of the following system remains to be proved.

$$\begin{aligned} &\ddot{\bar{\alpha}}(t) \approx (-\eta + \gamma\dot{\bar{\alpha}}^2(t))\sin(\bar{\alpha}(t)) - \xi\dot{\bar{\alpha}}(t) \ \ for\ t > T_{ss}, \\ &\bar{\alpha}(T_{ss}) \neq 0\,,\ \ \dot{\bar{\alpha}}(T_{ss}) \neq 0 \end{aligned} \quad \ldots(24)$$

At first, to understand the behaviour of the dynamics (24), it is supposed that there is no damping ratio ($\xi = 0$). The approximate relation between the peak value of gimbal angle $\bar{\alpha}_m$ (at $\dot{\bar{\alpha}} = 0$) and its maximum angular velocity $\dot{\bar{\alpha}}_m$ (at $\bar{\alpha} = 0$) are formulated here. Using the transformation $\ddot{\bar{\alpha}} = \dot{\bar{\alpha}}d\dot{\bar{\alpha}}/d\bar{\alpha} = d\dot{\bar{\alpha}}^2/2d\bar{\alpha}$ and by integrating Equation (24) from point ($\bar{\alpha} = 0,\ \dot{\bar{\alpha}} = \dot{\bar{\alpha}}_m$) to ($\bar{\alpha} = \bar{\alpha}_m,\ \dot{\bar{\alpha}} = 0$) the mentioned relation between $\bar{\alpha}_m$ and $\dot{\bar{\alpha}}_m$ is obtained in Equation (25).

$$\begin{aligned} &\frac{-1}{2}\frac{d\dot{\bar{\alpha}}^2}{\eta - \gamma\dot{\bar{\alpha}}^2(t)} \approx \sin(\bar{\alpha}(t))d\bar{\alpha} \overset{\int}{\Rightarrow} \frac{1}{2\gamma}\,Ln(\eta - \gamma\dot{\bar{\alpha}}^2)\Big|_{\dot{\bar{\alpha}}_m}^{0} \approx -\cos(\bar{\alpha})|_0^{\bar{\alpha}_m} \\ &\Rightarrow \dot{\bar{\alpha}}_m^2 \approx \frac{\eta}{\gamma}(1 - \exp\left[2\gamma(\cos(\bar{\alpha}_m) - 1)\right]) \end{aligned} \quad \ldots(25)$$

In the absence of the jet damping effect, Equation (25) gives the relation between the amplitude of gimbal angle $\bar{\alpha}_m$ and its rate amplitude $\dot{\bar{\alpha}}_m$ for the oscillatory behaviour of the dynamics Equation (24). In the other words, for $\xi = 0$ the maximum rates $\dot{\bar{\alpha}}_m$ (at $\bar{\alpha} = 0$) is only a function of maximum amplitude $\bar{\alpha}_m$ (at $\dot{\bar{\alpha}} = 0$) and does not converge to zero as time tends to infinity. Note that the condition (8) and the mission parameters can hold the condition $\gamma\dot{\bar{\alpha}}_m^2 < \eta$.

Theorem 1: in the presence of the jet damping ($\xi \neq 0$), the dynamics in Equation (24) is stable and $\bar{\alpha}(t) \to 0$ and $\dot{\bar{\alpha}}(t) \to 0$ as $t \to \infty$.

Proof: at first, three sequential points are defined in Equation (26) in order to be used as the bounds in the integrating of Equation (24). The aim is to show that $|\dot{\bar{\alpha}}(t)|_{\bar{\alpha}=0}$ will be decreased

https://doi.org/10.1017/aer.2017.51 Published online by Cambridge University Press

for each oscillation (or $|\dot{\bar{\alpha}}_3| < |\dot{\bar{\alpha}}_1|$)

$$P_1(t_1,\ \bar{\alpha}_1 = 0,\ \dot{\bar{\alpha}}_1),\ P_2(t_2,\ \bar{\alpha}_2,\ \dot{\bar{\alpha}}_2 = 0),\ P_3(t_3,\ \bar{\alpha}_3 = 0,\ \dot{\bar{\alpha}}_3)\ for\ t_1 < t_2 < t_3 \quad \ldots(26)$$

Using the transformations $\ddot{\bar{\alpha}} = \dot{\bar{\alpha}} d\dot{\bar{\alpha}}/d\bar{\alpha} = d\dot{\bar{\alpha}}^2/2d\bar{\alpha}$ and $\dot{\bar{\alpha}} d\bar{\alpha} = \dot{\bar{\alpha}}^2 dt$, and integrating of Equation (24) from P_1 to P_3, the following result is obtained in which reduction of the magnitude of $|\dot{\bar{\alpha}}(t)|_{\bar{\alpha}=0}$ is shown as time tends to infinity.

$$\begin{aligned} &\frac{1}{2\gamma} Ln(\eta - \gamma\dot{\bar{\alpha}}^2)\Big|_{\dot{\bar{\alpha}}_1}^{\dot{\bar{\alpha}}_3} = -\cos(\bar{\alpha})|_{\bar{\alpha}_1}^{\bar{\alpha}_3} + \sigma^2 \Rightarrow Ln\left(\frac{\eta-\gamma\dot{\bar{\alpha}}_3^2}{\eta-\gamma\dot{\bar{\alpha}}_1^2}\right) = 2\gamma\sigma^2 \\ &\Rightarrow \frac{\eta-\gamma\dot{\bar{\alpha}}_3^2}{\eta-\gamma\dot{\bar{\alpha}}_1^2} = \exp(2\gamma\sigma^2) > 1 \ \Rightarrow \left|\dot{\bar{\alpha}}_3(t_3)\right|_{\bar{\alpha}=0} < \left|\dot{\bar{\alpha}}_1(t_1)\right|_{\bar{\alpha}=0} for\ t_1 < t_3, \end{aligned} \quad \ldots(27)$$

where $\sigma^2 = \xi \int_{t_1}^{t_3} \frac{\dot{\bar{\alpha}}^2}{\eta-\gamma\dot{\bar{\alpha}}^2} dt > 0$.

Therefore, it can be claimed that by increasing the time $t > t_n$ the $|\dot{\bar{\alpha}}(t)|_{\bar{\alpha}=0}$ will be small enough to conclude $-\eta + \gamma\dot{\bar{\alpha}}^2(t) \approx -\eta$, then the approximate form of the dynamics in Equation (24) is achieved as

$$\ddot{\bar{\alpha}}(t) \approx -\eta \sin(\bar{\alpha}(t)) - \xi\dot{\bar{\alpha}}(t)\ \ for\ t > t_n \quad \ldots(28)$$

The candidate Lyapunov function is introduced as

$$V = \eta(1 - \cos(\bar{\alpha}(t))) + \frac{\dot{\bar{\alpha}}(t)^2}{2}. \quad \ldots(29)$$

The time derivative of V along the dynamics (28) is

$$\dot{V} \approx -\xi\dot{\bar{\alpha}}^2(t) < 0 \quad \ldots(30)$$

Because the set $(\dot{\bar{\alpha}} = 0,\ \bar{\alpha} \neq 0)$ is not a stable set for the dynamics (28), then from Equation (30), the stability of the error dynamics (28) can be easily concluded.

3.3.2 Numerical simulation

In this subsection, the performance of the nonlinear closed-loop system proven previously is illustrated. In addition to the parameters used in subsection 3.2.2, the parameters which are needed here are selected as $T_{ss} = 3\,s$ and $\lambda = 2.5/T_{ss} = 0.83/s$.

The body and the gimbal angle are presented in Fig. 8 while they are converging to $\theta_{eq} = -3.055^0$ and $\alpha_{eq} = 3.055^0$, respectively. Convergence of the thrust vector deviation can be observed in Fig. 9. Spacecraft velocity change along the two inertial directions is shown in Fig. 10. The velocity change along the axis X_I is $\Delta v_x = 99.97 m/s$ and the wasted velocity change is $\Delta v_w = 2.0\text{m/s}$.

The advantages of using the proposed nonlinear controller in comparison with using the linear controller are:

1. Smaller overshoot of the body attitude during the transient response (the damped behaviour) is achieved.

https://doi.org/10.1017/aer.2017.51 Published online by Cambridge University Press

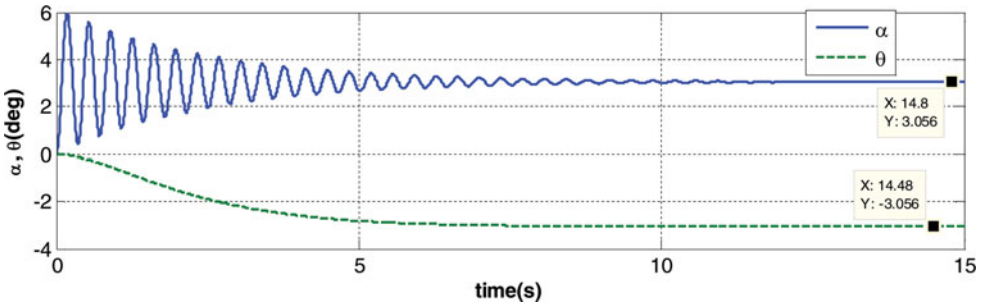

Figure 8. (Colour online) Spacecraft body attitude (θ) and gimbal angle (α) when using a nonlinear controller.

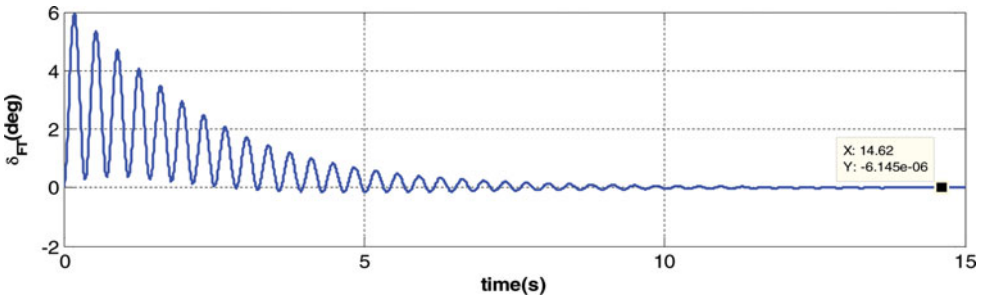

Figure 9. (Colour online) Thrust vector deviation (δ_{FT}) from the desired inertial direction (X_I) when using a nonlinear controller.

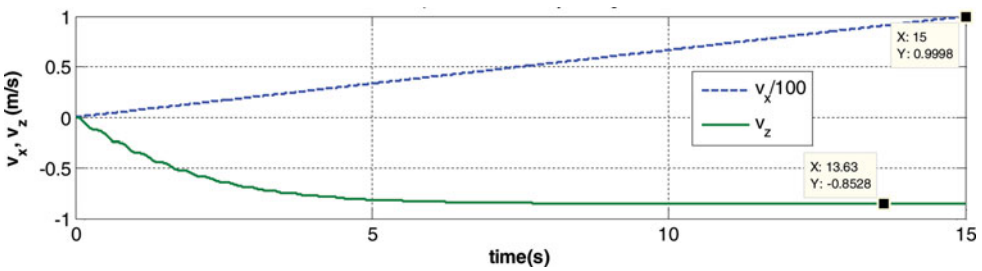

Figure 10. (Colour online) Spacecraft velocity change along the two inertial directions X_I and Z_I.

2. Due to smaller deviation of the body attitude and consequently a smaller deviation of the thrust vector, the wasted velocity change is become smaller.
3. The stability of the nonlinear closed-loop system is illustrated.

Although there are advantages, some weaknesses can be seen in this method: 1) in the steady-state response of the body attitude, gimbal angle deviation is not completely eliminated and is oscillating during the burning time, and 2) the control action in steady-state mode is not zero while it is also oscillating.

The important idea presented in the next subsection is to derive a control law based on the combination of the linear and nonlinear controllers in which only the advantages of the two mentioned controllers are included and their shortcomings are excluded.

https://doi.org/10.1017/aer.2017.51 Published online by Cambridge University Press

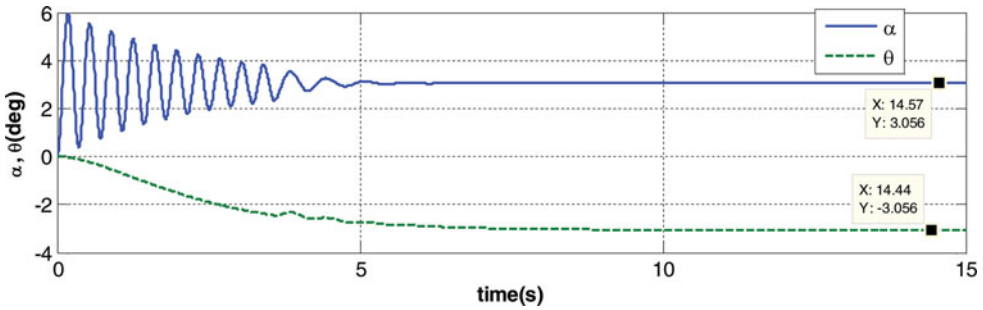

Figure 11. (Colour online) Spacecraft body attitude (θ) and gimbal angle (α) when using a combined controller.

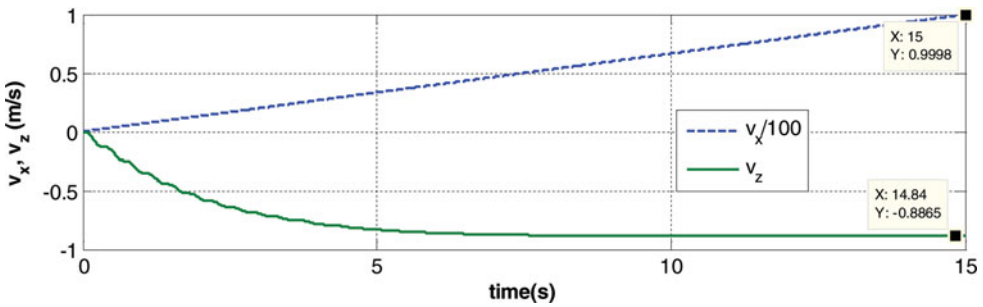

Figure 12. (Colour online) Spacecraft velocity change along the two inertial directions X_I and Z_I when using a combined controller.

3.4 Combined linear and nonlinear controller

The purpose of this subsection is to combine the mentioned linear and nonlinear controllers with the aim of utilising their advantages and excluding their weaknesses. The expectation is to have a better controller than the two others. Moreover, the control effort in the steady-state mode is an important criterion that will be compared with the other thrusting methods.

3.4.1 Controller design

There are many complex methods to combine two or more control laws, but in this paper a simple combination law is employed. The combined control logic works according to the following model:

$$u_{com} = (1 - \exp(-a_c t))\, u_{lin} + \exp(-a_c t)\, u_{nonl} \ , \qquad \ldots (31)$$

where u_{com} denotes the combined control input, and u_{lin} and u_{nonl} are the linear and nonlinear control law in Equations (17) and (19), respectively. a_c is a constant to tune the switching rate between the two controllers; here it is chosen as 0.25. During the burning, for t < 1.2 Tss, only u_{nonl} acts as the control input and for t > 1.2 Tss, u_{com} is applied.

3.4.2 Numerical simulation

The time response specifications are illustrated in Figs. 11 and 12. The velocity change along the axis X_I is $\Delta v_x = 99.97 m/s$ and the wasted velocity change is $\Delta v_w = 2.0 \mathrm{m/s}$. It can

https://doi.org/10.1017/aer.2017.51 Published online by Cambridge University Press

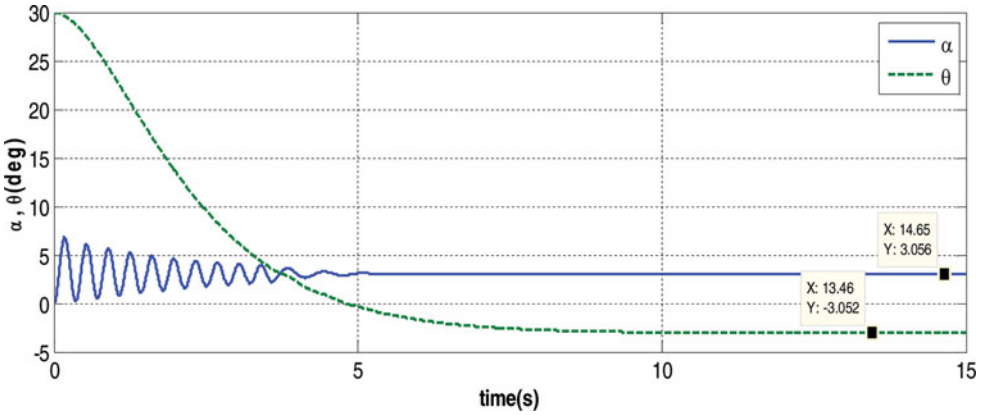

Figure 13. (Colour online) Spacecraft body attitude (θ) and gimbal angle (α) in the presence of high initial attitude deviation.

be easily seen that the nonlinear controller generates the transient response and the linear controller is working well in steady-state mode; in other words, the combined controller includes the advantages of the two aforementioned controllers. It should be noted that these results are for the misalignment $z_s = 4$ cm ($\alpha_{eq} = 3^0$); it is obvious that by decreasing the magnitude of the misalignment, all errors will be decreased and Δv_x converges to Δv_d.

In the following, closed-loop system performance is investigated in presence of high deviation in initial condition.

Based on the definition of the state-variables

$$\boldsymbol{X}(t) = \left[\bar{\theta}(t)\ \dot{\bar{\theta}}(t)\ \bar{\alpha}(t)\ \dot{\bar{\alpha}}(t)\right]^T = \left[\theta(t) - \theta_{eq}\ \dot{\bar{\theta}}(t)\ \alpha(t) - \alpha_{eq}\ \dot{\alpha}(t)\right]^T,$$

the vector of initial condition is

$$\boldsymbol{X}(0) = \left[\theta_0\ \dot{\theta}_0\ \alpha_0\ \dot{\alpha}_0\right]^T - \left[\theta_{eq}\ 0\ \alpha_{eq}\ 0\right]^T$$

In practice, before thrusting manoeuvre the attitude can be stabilised by using the simple control methods by which $\theta_0 = 0$, $\dot{\theta}_0 = 0$, $\alpha_0 = 0$ and $\dot{\alpha}_0 = 0$ can be achieved. Then using $\alpha_{eq} = z_s/x_s$ and $\theta_{eq} = -z_s/x_s$ the initial condition will be

$$\boldsymbol{X}(0) = \left[1\ 0\ -1\ 0\right]^T z_s/x_s\ ,$$

which is used in the previous simulations.

Against previous simulations, there is a simulation in Fig. 13 that shows the ability of the proposed method in presence of high deviation in initial condition (initial attitude deviation). To show this ability, in addition to the disturbance, a large deviation is considered for the body attitude as $\theta_0 = 30^0$. A well transient and steady-state response can be clearly seen in this simulation.

https://doi.org/10.1017/aer.2017.51 Published online by Cambridge University Press

4.0 DISCUSSION

The proposed thrusting method has some important merits in comparison with the RCS method. As shown before, in the steady-state mode of the proposed method, the large exogenous disturbance torque ($\tau_d = 42.13$Nm) is completely eliminated and rejected by a proper gimbal deflection while, in RCS method the mentioned disturbance always exist and should be rejected by a large active control torque that needs fuel consumption. It is assumed that four RCSs are located at the $z = \pm 30cm$ to create the control torque about the $\pm y_s$ axis, then the force of each RCS is calculated as $F_{RCS} = (\tau_d/0.3)/2 = 70.2$N. Using the I_{sp}=260s, the needed fuel is calculated about 0.8kg. As discussed in introduction section, in addition to the fuel consumption there are many disadvantages and limitations for using a RCS in a small spacecraft. It is obvious that for a longer time mission the more fuel consumption is needed but in the steady-state mode of the proposed method, control effort is zero because disturbances are successfully eliminated.

Many weaknesses and limitations of the basic (common) methods such as: spin-stabilisation and RCS are discussed in introduction section. At the following some major advantages of the proposed method in comparison with the spin-stabilisation, RCS, spin-stabilisation/RCS and TVC/RCS are summarised as:

1) Spin-stabilisation is just able to attenuate the exogenous disturbance effects but is not able to reject the disturbance caused by thrust vector misalignment, while in the proposed method the mentioned disturbance can be completely eliminated and rejected by a proper gimbal deflection at the steady-state mode.
2) When only the RCS method is employed, the disturbance torque rejection is accompanied by high control effort and fuel consumption during all of the burning time. But in the proposed method the control effort is zero in steady-state mode.
3) The proposed method does not need fuel consumption, stabilising spin and many complex components.
4) The combined TVC and RCS method is a powerful and accurate method but, for using in a small spacecraft it is not efficient and has many structural limitations.
5) Like as combined TVC and RCS, the combined spin-stabilisation and RCS is not suitable for a small spacecraft.

5.0 CONCLUSION

Although during an impulsive orbital manoeuvre a thrust vector misalignment generates a high level disturbance torque, an active control torque larger than the disturbance level can be obtained by using the TVC scheme. Based on some assumptions and criteria the subject of this paper is defined and then the weaknesses and limitations of the previous thrusting methods are well discussed to show they are not the proper choices for satisfying the objects of this paper. The structure of the proposed method is based on only the gimbaled-TVC where, the other control systems such as RCSs and spin-stabilisation are not employed moreover, a gimbal actuator does not need fuel consumption.

The major objects of the proposed underactuated control system are considered as 1) a damped (or under-damped) behaviour without an overshoot can be achieved for the body attitude in the transient mode 2) show the stability of the nonlinear closed-loop system 3) after the transient time or in the steady-state mode, thrust vector deviation should be completely

https://doi.org/10.1017/aer.2017.51 Published online by Cambridge University Press

eliminated 4) The control action in the steady-state mode remains zero while a high level exogenous disturbance can be completely rejected 5) near the equilibrium point, the closed-loop system converges to the steady-state mode very fast. To satisfy the mentioned objects, a linear controller is designed which has a good performance in the steady-state mode and then a nonlinear controller is proposed which is efficient to satisfy the transient mode objects. Since each of the linear and nonlinear controllers are just suitable for one mode (transient or steady-state), a new control law based on the combination of them is derived to satisfy both of the transient and steady-state modes objects, simultaneously. In the combined controller, the lacks of the linear and nonlinear controllers are excluded in a good manner. The attitude and thrust vector stabilisation along with full disturbance rejection are achieved where the maximum amplitude of the gimbal angle remains bounded in an acceptable range. Moreover, the good performance of the proposed method in presence of the high initial attitude deviation is illustrated.

A quantitative comparison to the RCS method is given to show the ability and effectiveness of the proposed method in sustained operation. It is shown that the proposed method has some advantages in comparison with the spin-stabilisation, RCS, spin-stabilisation/RCS and TVC/RCS. Considering the disadvantages of the other control methods, the proposed method can be very useful for an impulsive orbital manoeuvre of a small spacecraft, especially for missions with a long burning time.

An important application of the proposed method can be transferring the space debris (junk) to the deep space because; the other methods (such as spin-stabilisation and RCS) are not efficient and applicable for this mission.

REFERENCES

1. ORR, J.S. and SHTESSEL, Y.B. Lunar spacecraft powered descent control using higher-order sliding mode techniques, *J Franklin Institute*, 2012, **349**, (2), pp 476-492.
2. SOUZA, M. et al. A discussion on the effects of thrust misalignments on orbit transfers, Proceedings of the XXI Congresso Nacional de Matem tica Aplicada e Computacional, 1998, Caxambu, MG, Brazil.
3. NOLL, R. Spacecraft attitude control during thrusting maneuvers, NASA SP-8059, 1971.
4. KOUHI, H. et al. Retrofiring control method via combination of a 1DoF gimbaled thrust vector control and spin-stabilisation, *Proceedings of the Institution of Mechanical Engineers, Part G: Journal of Aerospace Engineering*, 2016. doi: 10.1177/0954410016650909.
5. OLDENBURG, J.A. and TRAGESSER, S.G. Minimizing the effects of transverse torques during thrusting for spin-stabilized spacecraft, *J Guidance, Control, and Dynamics*, 2002, **25**, (3), pp 591-595.
6. THIENEL, J.K. and MARKLEY, F.L. Comparison of angular velocity estimation methods for spinning spacecraft, Advances in Astronautical Science," AAS/AIAA Guidance, Navigation, and Control Conference, 2011, Portland, Oregon.
7. HU, X. and GONG, S. Flexibility influence on passive stability of a spinning solar sail, *Aerospace Science and Technology*, 2016, **58**, pp 60-70.
8. MEYER, R. Coning instability of spacecraft during periods of thrust, *J Spacecraft and Rockets*, 1996, **33**, (6), pp 781-788.
9. JANSSENS, F.L. and VAN DER HA, J.C. Stability of spinning satellite under axial thrust and internal mass motion, *Acta Astronautica*, 2014, **94**, (1), pp 502-514.
10. MARTIN, K.M. and LONGUSKI, J.M. Velocity pointing error reduction for spinning, thrusting spacecraft via heuristic thrust profiles, *J Spacecraft and Rockets*, 2015, **52**, (4), pp 1268-1272.
11. CLOUTIER, G. Resonances of a two-DOF system on a spin-stabilized spacecraft, *AIAA J*, 1976, **14**, (1), pp 107-109.

12. MEEHAN, P. and ASOKANTHAN, S. Control of chaotic motion in a spinning spacecraft with a circumferential nutational damper, *Nonlinear Dynamics*, 1998, **17**, (3), pp 269-284.
13. CLOUTIER, G.J. Nutation damper instability on spin-stabilized spacecraft, *AIAA J*, 1969, **7**, (11), pp 2110-2115.
14. TSIOTRAS, P. and LONGUSKI, J.M. Spin-axis stabilization of symmetric spacecraft with two control torques, *Systems & Control Letters*, 1994, **23**, (6), pp 395-402.
15. CHILDS, D.W. Fuel-optimal direction-cosine attitude control for spin-stabilized axisymmetric spacecraft. *J Spacecraft and Rockets*, 1970, **7**, (12), pp 1481-1483.
16. CHILDS, D.W., TAPLEY, B.D. and FOWLER, W.T. Suboptimal attitude control of a spin-stabilized axisymmetric spacecraft. *IEEE Transactions on Automatic Control*, 1969, **14**, (6), pp 736-740.
17. GUI, H. and VUKOVICH, G. Robust adaptive spin-axis stabilization of a symmetric spacecraft using two bounded torques, *Advances in Space Research*, 2015, **56**, (11), pp 2495-2507.
18. REYHANOGLU, M. and HERVAS, J.R. Nonlinear dynamics and control of space vehicles with multiple fuel slosh modes, *Control Engineering Practice*, 2012, **20**, (9), pp 912-918.
19. BANDYOPADHYAY, B., KURODE, S. and GANDHI, P. Sliding mode control for slosh-free motion-A class of underactuated system. *Int J Advanced Mechatronic Systems*, 2009, **1**, (3), pp 203-213.
20. PETERSON, L.D., CRAWLEY, E.F. and HANSMAN, R.J. Nonlinear fluid slosh coupled to the dynamics of a spacecraft, *AIAA J*, 1989, **27**, (9), pp 1230-1240.
21. SHEKHAWAT, A., NICHKAWDE, C. and ANANTHKRISHNAN, N. modelling and stability analysis of coupled slosh-vehicle dynamics in planar atmospheric flight, Proceedings of the 44th AIAA Aerospace Sciences Meeting and Exhibit, 2006, Reno, Nevada, US.
22. HERVAS, J.R. and REYHANOGLU, M. Thrust-vector control of a three-axis stabilized upper-stage rocket with fuel slosh dynamics, *Acta Astronautica*, 2014, **98**, pp 120-127.
23. RUBIO HERVAS, J. and REYHANOGLU, M. Thrust-vector control of a three-axis stabilized upper-stage rocket with fuel slosh dynamics, *Acta Astronautica*, 2014, **98**, pp 120-127.
24. KISHORE, W.A. et al. Control allocation for an over-actuated satellite launch vehicle, *Aerospace Science and Technology*, 2013, **28**, (1), pp 56-71.
25. HALL, R.A. et al. Design and stability of an on-orbit attitude control system using reaction control thrusters, AIAA Guidance, Navigation, and Control Conference, San Diego, California, US, 2016.
26. YEH, F.-K. Sliding-mode-based contour-following controller for guidance and autopilot systems of launch vehicles, *Proceedings of the Institution of Mechanical Engineers, Part G: Journal of Aerospace Engineering*, 2013, **227**, (2), pp 285-302.
27. WIDNALL, W.S. The minimum-time thrust-vector control law in the Apollo lunar-module autopilot, *Automatica*, 1970, **6**, (5), pp 661-672.
28. WANG, Z. et al. Thrust vector control of upper stage with a gimbaled thruster during orbit transfer. *Acta Astronautica*, 2016.
29. RIZVI, F. and WEITL, R.M. Characterizing limit cycles in the cassini thrust vector control system, *J Guidance, Control, and Dynamics*, 2013, **36**, (5), pp 1490-1500.
30. MILLARD, J. AND REED, B. Implementation of the orbital maneuvering system engine and thrust vector control for the European service module, 50th AIAA/ASME/SAE/ASEE Joint Propulsion Conference, Cleveland, Ohio, US, 2014.
31. KONG, F., JIN, Y. and KIM, H.D. Thrust vector control of supersonic nozzle flow using a moving plate, *J Mechanical Science and Technology*, 2016, **30**, (3), pp 1209-1216.
32. SPERBER, E., FU, B. and EKE, F. Large angle reorientation of a solar sail using gimballed mass control, *J Astronautical Sciences*, 2016, pp 1-21.
33. KOUHI, H., MANSOUR, K., FANI SABERI, F., and SHAHRAVI, M. Robust control of a spin-stabilized spacecraft via a 1DoF gimbaled-thruster and two reaction wheels, *ISA Transactions*, 2017, **66**, 310–324.
34. FELICETTI, L. et al. Adaptive thrust vector control during on-orbit servicing, *Proceedings of AIAA SPACE 2014 Conference and Exposition*, paper AIAA-2014-4341, 2014, San Diego, California, US.
35. VAN DER HA, J.C. and JANSSENS, F.L. Jet-damping and misalignment effects during solid-rocket-motor burn, *J Guidance, Control, and Dynamics*, 2005, **28**, (3), pp 412-420.
36. VAN DER HA, J.C. Lessons learned from the dynamical behaviour of orbiting satellites, *Acta Astronautica*, 2015, **115**, pp 121-137.

https://doi.org/10.1017/aer.2017.51 Published online by Cambridge University Press

37. CHEN, W.-H. Nonlinear disturbance observer-enhanced dynamic inversion control of missiles, *J Guidance, Control, and Dynamics*, 2003, **26**, (1), pp 161-166.
38. WU, G. and MENG, X. Nonlinear disturbance observer based robust backstepping control for a flexible air-breathing hypersonic vehicle, *Aerospace Science and Technology*, 2016, **54**, pp 174-182.

https://doi.org/10.1017/aer.2017.51 Published online by Cambridge University Press